

Provided for non-commercial research and education use.
Not for reproduction, distribution or commercial use.



This article appeared in a journal published by Elsevier. The attached copy is furnished to the author for internal non-commercial research and education use, including for instruction at the authors institution and sharing with colleagues.

Other uses, including reproduction and distribution, or selling or licensing copies, or posting to personal, institutional or third party websites are prohibited.

In most cases authors are permitted to post their version of the article (e.g. in Word or Tex form) to their personal website or institutional repository. Authors requiring further information regarding Elsevier's archiving and manuscript policies are encouraged to visit:

<http://www.elsevier.com/copyright>



Contents lists available at ScienceDirect

Biochimica et Biophysica Acta

journal homepage: www.elsevier.com/locate/bbamem

Plant actin controls membrane permeability

Petra Hohenberger^a, Christian Eing^b, Ralf Straessner^b, Steffen Durst^a, Wolfgang Frey^b, Peter Nick^{a,*}^a Botanical Institute, Karlsruhe Institute of Technology, Kaiserstr. 2, 76128 Karlsruhe, Germany^b Institute for Pulsed Power and Microwave Technology (IHM), Karlsruhe Institute of Technology, Campus Nord, 76344 Eggenstein-Leopoldshafen, Germany

ARTICLE INFO

Article history:

Received 23 March 2011

Received in revised form 26 May 2011

Accepted 27 May 2011

Available online 6 June 2011

Keywords:

Actin

Plant cell

Pulsed electric field

Tobacco BY-2

Total internal reflection microscopy

ABSTRACT

The biological effects of electric pulses with low rise time, high field strength, and durations in the nanosecond range (nsPEFs) have attracted considerable biotechnological and medical interest. However, the cellular mechanisms causing membrane permeabilization by nanosecond pulsed electric fields are still far from being understood. We investigated the role of actin filaments for membrane permeability in plant cells using cell lines where different degrees of actin bundling had been introduced by genetic engineering. We demonstrate that stabilization of actin increases the stability of the plasma membrane against electric permeabilization recorded by penetration of Trypan Blue into the cytoplasm. By use of a cell line expressing the actin bundling WLIM domain under control of an inducible promoter we can activate membrane stabilization by the glucocorticoid analog dexamethasone. By total internal reflection fluorescence microscopy we can visualize a subset of the cytoskeleton that is directly adjacent to the plasma membrane. We conclude that this submembrane cytoskeleton stabilizes the plasma membrane against permeabilization through electric pulses.

© 2011 Elsevier B.V. All rights reserved.

1. Introduction

Numerous biotechnological and medical applications require the transport of large molecules across the plasma membrane, but only few biomolecules can spontaneously pass the plasma membrane. During evolution, specific patterns of carriers and transporters have developed that facilitate the import of those substrates that are required for the corresponding cellular function. To alter these cell-type dependent patterns for technical applications is often difficult and often poses serious constraints to bioengineering. Artificial induction of membrane permeability by pulsed electric fields (PEFs) has been used successfully to introduce large molecules into living cells (for reviews see [1–4]), to extract cell ingredients [5–7] or to inactivate microorganisms without the help of heat [8–11]. In classical electroporation, the duration of the pulsed electric fields is in the range of micro- to even milliseconds. The used amplitudes of the electric field permeabilize the membrane irreversibly (for a recent review see [12]). However, when the cells are exposed to so called nanosecond pulsed electric fields (nsPEFs), i.e. electric pulses of high field strength (up to 300 kV cm⁻¹), low risetime, and simultaneously very short pulse durations (ns range), the electric field can penetrate

into the cell before it is dissipated by charging of the plasma membrane [13], which allows to manipulate intracellular targets, such as membranes of organelles. The biological effects of these nsPEFs differ from those induced by classical electroporation and have attracted considerable interest, because they can induce specific cellular responses such as calcium release from intracellular stores [14,15], externalization of phosphatidylserine [16], and apoptosis [17,18], which has already been employed successfully for tumor therapy [19]. However, the cellular mechanisms triggering these cellular responses are still far from being understood.

The cytoskeleton is important as architectural component of animal cells. In addition, it plays a central role in the dynamics and organization of the plasma membrane and therefore represents a key candidate for the action of pulsed fields. Microtubules, for instance, due to their strongly negatively charged carboxyterminus and their long axes are electrically highly polar (electric dipole momentum in the range of 1000 Debye [20]). In fact, in mammalian cells, elimination of microtubules by colchicine has been reported to delay the recovery from electric permeabilization [21,22]. However, there is mounting evidence for a role of actin as well. The extensibility of the membrane probed with optical tweezers was found to increase in mesenchymal stem cells and osteoblasts in response to electric currents accompanied by a decrease in the number of actin filaments and the decoration of actin by tethering proteins [23]. In melanoma cells that are key targets for nsPEF-based curative treatment, actin (visualized by rhodamine-phalloidin) was disrupted, which was linked to altered activation of caspases, central regulators of apoptosis [24].

In our previous work, we have analyzed the cellular effects of nsPEFs on plant cells using tobacco cell lines, where the cytoskeleton

Abbreviations: nsPEFs, nanosecond pulsed electric fields; TIRF, total internal reflection fluorescence

* Corresponding author. Tel.: +49 721 608 2144 (secretary 2142); fax +49 721 608 4193.

E-mail addresses: petra.hohenberger@kit.edu (P. Hohenberger), christian.eing@ihm.fzk.de (C. Eing), ralf.straessner@kit.edu (R. Straessner), steffen.durst@bio.uni-karlsruhe.de (S. Durst), wolfgang.frey@kit.edu (W. Frey), peter.nick@bio.uni-karlsruhe.de (P. Nick).

(microtubules, actin filaments) or the endomembrane system was fluorescently tagged by the Green Fluorescent Protein [25]. When the response of these marker lines to nsPEFs were followed by confocal laser scanning microscopy, a rapid disintegration of the cytoskeleton in the cell cortex was observed, followed by contraction of actin filaments towards the nucleus, and disintegration of the nuclear envelope. These responses were accompanied by irreversible permeabilization of the plasma membrane manifest as uptake of Trypan Blue. By pretreatment with the actin-stabilizing drug phalloidin, both the actin responses as well as the irreversible permeabilization of the membranes could be suppressed.

To investigate a potential role of actin filaments for membrane permeability, we used, in the present work, the approach to manipulate actin organization by genetic engineering. We generated tobacco cell lines, where actin was bundled (mimicking a treatment with phalloidin) in consequence of a constitutive overexpression of specific actin-binding proteins (plant fimbrin, mouse talin) or by inducible expression of the actin-bundling WLIM1 protein. We followed membrane permeability in response to both nsPEFs and conventional electroporation recorded by uptake of the membrane-impermeable dye Trypan Blue over time and recorded dose–response functions by variation of pulse numbers. To visualize the submembrane cytoskeleton, we imaged the submembrane cytoskeleton by Total-Internal-Reflection Microscopy (TIRF).

2. Material and methods

2.1. Cell lines

The tobacco cell line BY-2 (*Nicotiana tabacum* L. cv. Bright Yellow 2) was the source line for all transgenic lines used in this study and has been derived from pith parenchyma cells [26]. In addition to the non-transformed BY-2 wild type, transgenic lines were used over-expressing either the actin-binding domain 2 of plant fimbrin in fusion with GFP under control of the constitutive CaMV 35S promoter [27], the actin-binding domain of mouse talin in fusion with GFP under control of the constitutive CaMV 35S promoter [28], or the actin-bundling LIM-domain in fusion with GFP under control of a glucocorticoid-inducible promoter [28]. In addition, a transgenic BY-2 line expressing the actin-binding Lifeact peptide in fusion with the VENUS fluorescent protein [30] under control of a constitutive CaMV 35S promoter, and a transgenic line expressing the β -tubulin AtTuB6 from *Arabidopsis thaliana* in fusion with GFP [31] under control of the constitutive CaMV 35S promoter were generated as described in Ref. [27].

2.2. Plant cell culture

The tobacco cells were cultivated in liquid medium (4.3 g/l Murashige and Skoog salts, Duchefa, Haarlem, The Netherlands, 30 g/l sucrose, 200 mg/l KH_2PO_4 , 100 mg/l inositol, 1 mg/l thiamine and 0.2 mg/l 2,4-D, pH 5.8 at 25 °C in the dark on an orbital shaker at 150 rpm. Cells were subcultivated weekly by inoculation of 1 ml cells into 30 ml fresh media. The media for the transgenic cell lines were complemented with either 30 mg/l hygromycin (WLIM–GFP, Lifeact–VENUS), with 25 mg/l kanamycin (mTalin–GFP), 50 mg/l kanamycin (AtTuB6–GFP), or with 100 mg/l kanamycin (FABD2–GFP), respectively. To induce the WLIM–GFP, cells were incubated for 24 h with 10 μM dexamethasone (Sigma–Aldrich, Neu-Ulm, Germany), diluted from a 10 mM stock.

2.3. Protoplast isolation

Protoplasts were generated following a published protocol [32] with minor modifications. BY-2 cells (30 ml per sample) were harvested by centrifugation 3 days after subcultivation (3000 g,

10 min, room temperature) and digested in 10 ml 0.4 M mannitol complemented with 1% cellulase, 0.1% pectolyase, and 0.5% BSA (pH 5.5) over night at 25 °C under gentle agitation. Protoplasts were centrifuged (100 g, 5 min, room temperature) and washed three times with 0.4 M mannitol and once additionally with electroporation buffer (5 mM MES, 70 mM KCl, 0.3 M mannitol, pH 5.8). After determining cell density using a Fuchs-Rosenthal counting chamber they were resuspended in the electroporation buffer to a density of $1.5 \cdot 10^6$ cells/ml.

2.4. Electroporation

500 μl of the protoplast suspension were used for electroporation (electroporation cuvette with 2 mm electrode gap, long electrode, Peqlab, Germany) in a Gene Pulser (Xcell, Bio-Rad München, Germany). Different numbers of square pulses with 800 V/cm, in some experiments with 1600 V/cm, were administered (pulse duration 3 ms, pulse intervals 1 s). Immediately after pulsing, 500 μl of ice cold electroporation buffer were added, and protoplasts centrifuged (100 g, 5 min, room temperature), and resuspended in 500 μl 0.4 M mannitol. In one experimental variant, Trypan Blue (final concentration 0.002 w/v%, Sigma–Aldrich, Neu-Ulm, Germany) was added at different time points after the pulse, the protoplasts were collected by centrifugation (100 g, 5 min, room temperature), washed with 0.4 M mannitol and immediately evaluated microscopically. In a second experimental variant, the protoplasts were pulsed in presence of Fluorescein (0.1% w/v, Sigma–Aldrich, Neu-Ulm, Germany), collected by centrifugation (100 g, 5 min, room temperature), washed with 0.4 M and immediately evaluated microscopically.

2.5. nsPEFs

The set-up to administer nsPEFs has been described previously [25]. To ensure that the conductivity of the cell suspension was appropriate for the nsPEF-treatment, the cells were sedimented, and the supernatant culture medium replaced by an equal volume of charging buffer (125 mM KCl, 5 mM $\text{CaCl}_2 \cdot 2\text{H}_2\text{O}$, 5 mM $\text{MgCl}_2 \cdot 6\text{H}_2\text{O}$, 150 mM sorbitol, and 1 mM TRIS, pH 7.2). For each experiment, 30 μl of the suspension were transferred between the two titanium electrodes of the microelectrode array that was fixed on a standard microscope slide and covered with a coverslip. The gap distance between the electrodes was 300 μm , with an electrode height of 75 μm . After filling, the microelectrode array containing the cells was fixed to a receptacle mounted on the linear motion stage of the microscope. The voltage applied to the electrodes was delivered by a square pulse generator with a risetime of 800 ps, a pulse duration of 10 ns, and a maximum output voltage of 1 kV (IPG 2501, HILO-Test, Karlsruhe, Germany). The waveforms of the voltage impulse were monitored with a 600 MHz oscilloscope (WaveRunner 64Xi, LeCroy Corporation, Chestnut Ridge, NY, USA) in combination with a Philips probe (PM 8931, Philips, The Netherlands). Using the maximum output voltage of the square pulse generator (1 kV) an effective electric field strength of 33 kV/cm could be generated.

2.6. Microscopy

The response to the nsPEFs was recorded by confocal laser scanning microscopy (TCS SP1, Leica, Bensheim, Germany) placing the focal plane into the cell center with respect to the z-axis and keeping the pinhole narrow (1 μm width using a 63 \times objective). A dual wavelength configuration was employed using the ArKr-laser lines 488 and 564 nm, beam splitter DD, and emission filters LP 515 or OG590, respectively, and a 4-frame averaging algorithm. To assess membrane permeability, the cells were mixed with an equal volume of 2.5% w/v Trypan Blue (Sigma), immediately before loading to the gap. Paired images of selected cells were recorded immediately prior

to the pulse treatment and 10 min after the pulse. In some cases, time series were imaged at 1-min intervals. The response to electroporation was monitored using an AxioImager Z.1 microscope (Zeiss, Göttingen, Germany) equipped with an ApoTome microscope slider for optical sectioning, and a cooled digital CCD camera (AxioCam MRm). The Trypan Blue signal was recorded through the filter set 43 HE (excitation at 550 nm, beam splitter at 570 nm, and emission at 605 nm), the Fluorescein signal through the filter set 38 HE (excitation at 470 nm, beam splitter at 495 nm, and emission at 525 nm), respectively, using a 63× plan apochromate oil-immersion objective. Images were processed and analyzed using the AxioVision software (Rel. 4.5; Zeiss).

For TIRF microscopy, protoplasts of transgenic tobacco cell lines were prepared at day 3 after subcultivation as described above. After washing, the protoplasts were resuspended in 0.4 M mannitol and analyzed subsequently using the iMIC Digital Microscope with TIRF condenser (TILL Photonics, Graefelfing, Germany). As light sources, a Polychrome V Monochromator and a Laser Line Combiner was used, the GFP signal was excited at 488 nm. The Live Acquisition Software (TILL Photonics) was used for image acquisition.

2.7. Quantification of membrane permeability

To quantify the uptake of Trypan Blue in the nsPEF experiment, the paired images were transformed into binary images using the Make Binary command of ImageJ (<http://rsb.info.nih.gov/ij/>), and then the image recorded prior to the pulse was subtracted from the image recorded 10 min after the pulse. Uptake of Trypan Blue was then quantified in relative units as integrated density over the cell file normalized by the integrated density prior to the pulse. The uptake of fluorescent tracers in the electroporation experiment (Fig. 3) was non-gradual. Whereas in some cells the signal was in the range of the unpulsed control, other cells were strongly fluorescent. Due to this discrete output in the response of individual cells, the number of fluorescent protoplasts was scored and their relative frequency used as measure to quantify uptake.

3. Theory

Actin organization represents an evolutionary conserved central element of apoptosis and programmed cell death in plants, fungi, and animal cells. Since the cytoskeleton has diversified during evolution, the molecular link between actin and apoptosis/programmed cell death differs partially between the kingdoms, but, as a common element, the transduction of external signals through the plasma membrane on actin organization and dynamics has been preserved [33]. The plasmamembrane–actin complex can, thus, be divided into two logical elements: (i) a link of the extracellular membrane surface through the membrane and (ii) a dynamic, regulated interaction between the inner surface of the plasma membrane and actin.

(i) A continuum between the cytoskeleton and the extracellular matrix is central for mechanosensing in animal cells (for review see [34]), and involves interaction between integrins and extracellular matrix proteins that harbor Arg–Gly–Asp (RGD) motives (for review see [35]). Plants seem to lack integrin homologues, but there is evidence for cytoskeletal reorganization in response to treatment with RGD peptides [36,37]. Here, treatment with RGD-peptides (that cannot permeate the membrane, but disrupt the interaction of the cytoskeleton with the plasma membrane through an unknown integrin-like protein) caused the disruption of cytoplasmic architecture and inhibited deplasmolysis indicating a loss of membrane integrity [37]. In *Chrysanthemum* cells, mechanosensing of the cytoskeleton could be impaired by treatment with RGD-peptides [37]. This evidence suggests signaling from the extracellular surface into the cell interior by unknown proteins that functionally replace animal integrins.

(ii) A regulated bidirectional link between actin and membrane topology has been demonstrated repeatedly as well. For instance, phosphorylation of a myosin light chain has been found to be necessary and sufficient for actin-dependent apoptotic membrane blebbing [38]. Conversely, the actin-binding N-WASP/WIP complex can transmit a signal from membrane curving upon the assembly of F-actin [39]. In plants, members of the actin-binding formin family contain a transmembrane domain and might tether actin filaments to the plasma membrane (for review see [40]). In fact, one member of this class, formin 5, was shown to mediate polar pollen tube growth by stimulating actin assembly from the subapical membrane [41], and recently was reported to act as cross-linker between actin and microtubules [42]. Moreover, the membrane-bound phospholipase D and its product phosphatidic acid (PA) are important regulators in the membrane–cytoskeleton interface of pollen tubes [43]. Interestingly, plant phospholipase D as well had originally been identified as membrane linker of plant microtubules [44]. Therefore, several lines of evidence support a close interaction between actin and microtubules at the plasma membrane of plants at specific domains that communicate with the exterior environment probably through conformational changes of so far unidentified transmembrane proteins.

4. Results

4.1. nsPEFs induce rapid permeabilization of the plasma membrane in living plant cells

To monitor the response of membrane permeability to nsPEFs, we used the membrane impermeable dye Trypan Blue in a cell line expressing the actin marker FABD2 in fusion with GFP. Trypan Blue emits red fluorescence upon activation by green light and thereby can be readily discriminated by dual-wavelength confocal microscopy from the GFP marker used to visualize actin filaments. In response to 5 pulses of 33 kV cm⁻¹, the red signal was observed to penetrate into the cell cortex during the first 10 min (Fig. 1A, B). Prior to pulsing, the cytoplasm appeared in green due to the GFP signal from the actin marker FABD2, and was clearly separated from the red Trypan Blue signal at the plasma membrane. 10 min after pulsing, the red signal had penetrated into the cytoplasm and merged with the green signal into a yellow overlay signal. Penetration was more pronounced at the cell pole as compared to the long flank of these cells that are clearly elongated. To quantify the penetration intensity, profiles were recorded for the Trypan Blue signal (Fig. 1C). The initial sharp peak at the plasma membrane was progressively replaced by a broader distribution with a decreasing peak and an increasing tail at the cytoplasmic side of the membrane. This effect was more pronounced in the cell pole and became detectable already from 1 min after pulsing, whereas it was generally weaker at the long side flanks of the cell and became detectable only from 3 min after pulsing.

4.2. Actin bundling stabilizes the plasma membrane against permeabilization by nsPEFs

Using the penetration of the Trypan Blue signal into the cytoplasm as a measure for membrane permeabilization, we constructed dose–response relations for a panel of transgenic lines and treatments that were connected with differential configurations of actin filaments (Fig. 2A). Confocal sections prior to pulsing and 10 min after pulsing were recorded and then subjected to quantitative image processing in order to assess the differential signal from Trypan Blue that had penetrated into the cytoplasm in response to the pulse treatment (Fig. 2A). We observed that the apparent thickness of the plasma membrane visualized by Trypan Blue differed depending on the degree of actin bundling (Fig. 2A). The plasma membrane appeared as thin line in the non-transformed wild type, slightly thicker in the actin

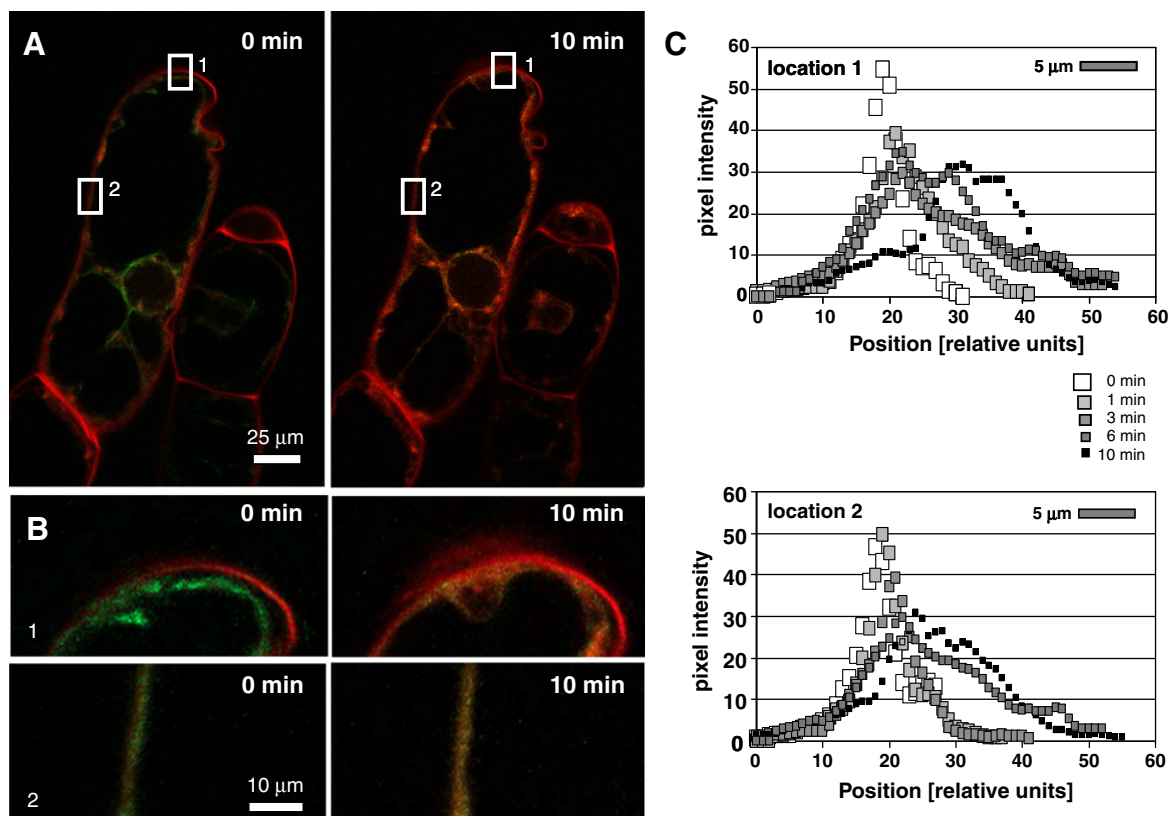


Fig. 1. Time course of membrane permeability in response to nsPEFs. Membrane permeability was followed by the uptake of Trypan Blue into tobacco BY-2 cells expressing the actin-binding domain of fimbrin in fusion with GFP. Cells were challenged with 5 pulses of 33 kV cm^{-1} and uptake followed by confocal laser-scanning microscopy. The electric field is directed bottom-up. A Confocal section in the cell center with a merge of the two channels collecting the Trypan Blue signal (red), and the signal for actin filaments (green) prior to (0 min) and 10 min after the pulse treatment. Note the yellow signal in the cytoplasmic strands tethering the nucleus and adjacent to the plasma membrane monitoring an overlap of the two signals. B close-ups of the cell pole (1) and the cell equator (2). C Pixel intensity profiles for the Trypan Blue signal collected at different time points after the pulse treatment in the cell pole (location 1) or the cell equator (location 2), highlighted in A. Pixel intensity has been corrected for bleaching during the experiment by using the corresponding GFP signals as reference (for details see [Material and methods](#)).

marker line FABD2–GFP, and was conspicuously expanded in the talin overexpressor line, where actin is constitutively bundled. By addition of the natural auxin indole acetic acid (IAA) to the talin overexpressor, a normal actin configuration with fine strands could be restored which was accompanied by a much thinner plasma membrane signal (Fig. 2A). Moreover, in a line expressing the non-bundling actin marker Lifeact in fusion with the VENUS-marker, the Trypan-Blue signal was indistinguishable from the non-transformed wild type, and the same was true for the WLIM-expressor line in the absence of dexamethasone (data not shown), whereas the plasma membrane signal became progressively thicker, when actin bundling was induced in the WLIM line by activating the promoter by the inducer dexamethasone (data not shown). To verify that the Trypan-Blue signal originated from the plasma membrane and not from the cell wall, we performed a double stain with Trypan Blue and the cell-wall dye Calcofluor White (Fig. 2A). The red signal from Trypan Blue and the blue signal from Calcofluor White were clearly separated in this control staining.

In the non-transformed wild type and the line expressing the non-bundling actin marker Lifeact in fusion with the VENUS-marker, the abundance of Trypan Blue penetrating into the cell increased with the number of pulses (33 kV cm^{-1} per pulse) reaching a plateau at 10 pulses (Fig. 2C). For the actin marker FABD2 in fusion with GFP causing a very mild bundling of actin filaments, the plateau was strongly reduced, and for the talin overexpressor, where actin is heavily bundled, there was hardly any response even for the highest pulse number of 20. To exclude any effect of transgene overexpression *per se*, we used the inducible WLIM line (Fig. 2D). In the absence of

inducer, the dose–response curve strongly resembled that of non-transformed wild type, after induction of the promoter by dexamethasone, the expression of WLIM causes progressive actin bundling [29]. This actin bundling, despite an identical genetical background, strongly reduced the permeability response to pulsing (Fig. 2D).

4.3. Actin bundling stabilizes the plasma membrane against electroporation

To test, whether the increased membrane stability in cells with bundled actin was restricted to nsPEFs, we tested conditions conventionally used for electroporation of plant cells (800 V cm^{-1} , 3 ms). We employed two configurations. 1. To monitor the time course for the response of membrane permeability, we pulsed protoplasts and added, after variable time intervals, Trypan Blue as reporter for membrane permeability. After washout of unbound Trypan Blue, the number of fluorescent protoplasts was scored (Fig. 3A). 2. To test, whether the response of membrane permeability was dependent on the total dose rather than on the number of pulses, the protoplasts were treated with sequential pulses of either 800 V cm^{-1} or 1600 V cm^{-1} in presence of the fluorescent reporter, and the result was scored 20 min after the pulse (Fig. 3D). For the second set-up, Fluorescein had to be used as reporter, because pulsing in the presence of Trypan Blue caused immediate lethality of the protoplasts (data not shown). In preparatory studies, frequency distributions were constructed over uptake intensity for both configurations and had revealed that uptake obeyed a clear all-or-none rule: the cells either did not accept any tracer or they were found

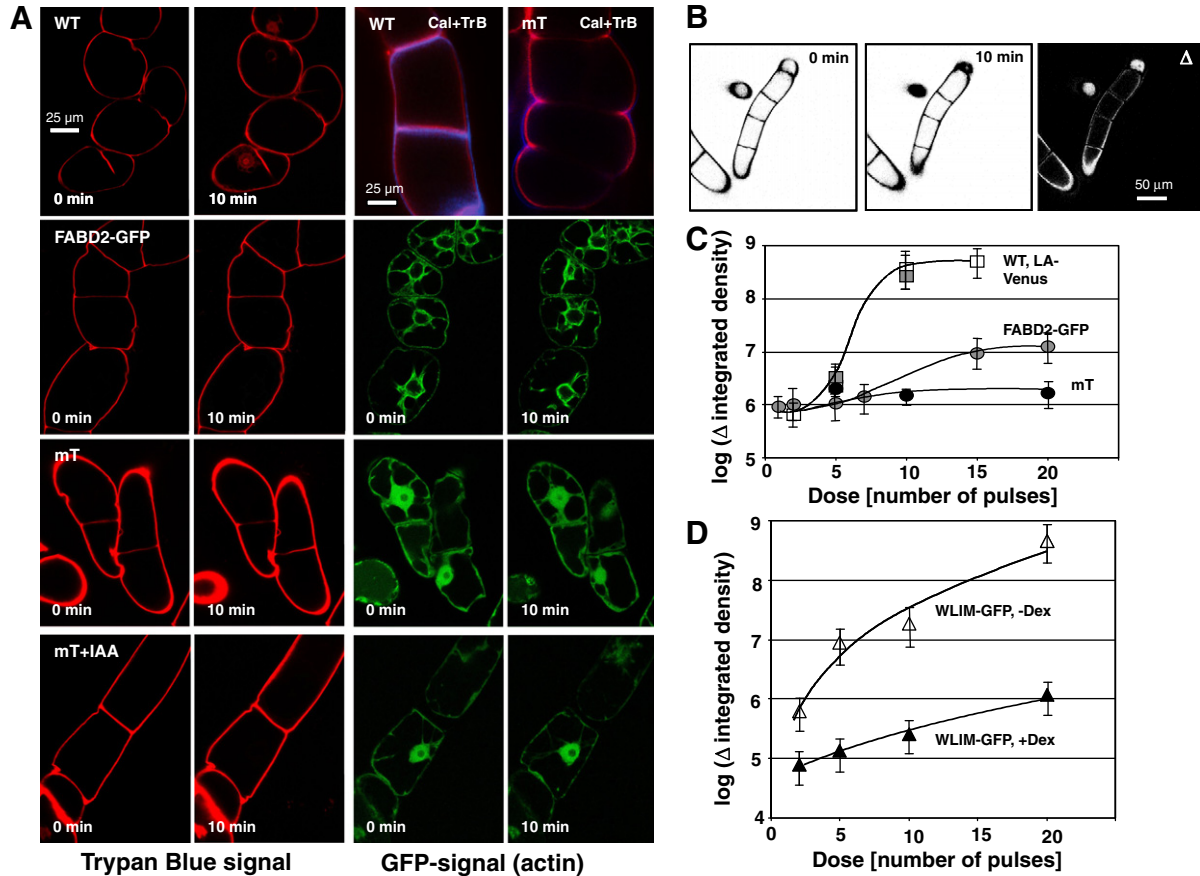


Fig. 2. Dose response of membrane permeability in response to nsPEFs upon manipulation of actin filaments. **A** Trypan Blue (red), and actin signal (recorded by GFP, green) prior to (0 min) and 10 min after treatment with 5 pulses of 33 kV cm^{-1} , field vector pointing bottom-up, in non-transformed wild type (WT), in cells overexpressing the actin-binding domain of fimbrin in fusion with GFP (FABD2-GFP), the actin-binding domain of mouse talin in fusion with GFP (mT), and the mT line after pretreatment with the auxin indole-3-acetic acid ($5 \mu\text{M}$ for 30 min prior to pulsing). Upper right image shows a double staining with Trypan Blue (TrpB, red) and the cellulose dye Calcofluor White (Cal, blue) in the WT and the mT line for comparison. **B** Quantification of TrpB uptake. Binary images of cells prior to and after the pulse treatment, differential image obtained by subtracting the image recorded prior to the pulse from the image recorded 10 min after the pulse. Uptake is quantified in relative units as integrated density over the cell file normalized by the integrated density prior to the pulse. **C** Dose response of TrpB uptake in relation to the number of pulses (33 kV cm^{-1} per pulse) recorded 10 min after pulsing in the non-transformed wild type (WT) versus lines expressing the non-invasive actin marker Lifeact in fusion with the VENUS fluorescent protein (LA-VENUS), the actin-binding domain of fimbrin in fusion with GFP (FABD2-GFP), and the actin-binding domain of mouse talin in fusion with GFP (mT). **D** As C, but for the inducible WLM-GFP either in the absence of the dexamethasone (DEX) inducer or after induction of WLM-GFP expression with $1 \mu\text{M}$ DEX for 12 h. Mean values of 20–30 individual cell files are scored along with the standard errors.

to be strongly fluorescent (data not shown). Due to this discrete output in the cellular response, the number of fluorescent protoplasts was scored and their relative frequency used as measure to quantify uptake. The time course of uptake in non-transformed wild-type cells followed a biphasic pattern with a peak between 30 and 60 min after pulse treatment, a trough between 60 and 90 min, and a second steady increase after 90 min (Fig. 3B). Those protoplasts that were observed to be strongly fluorescent at 60 min after the pulsing died soon afterwards (data not shown), i.e. the second steady increase was caused by protoplasts where at 60 min the fluorescent tracer had not penetrated yet.

In the next step, the response of non-transformed wild type was scored 2 h after pulsing and compared to that of cells where actin was bundled (by expression of FABD2 or mouse talin). The uptake was strongly reduced in the two lines, where actin was bundled (Fig. 3C) – this was even true for the lines expressing FABD2, where the bundling of actin was relatively mild.

For the test of dose-reciprocity (Fig. 3E), the response was scored 20 min after pulsing (in presence of the fluorescent reporter) and plotted as a function of electric energy density:

$$\Delta E = \sigma E^2 N \tau$$

with σ conductivity of the suspension, E intensity of the electric field, N number of pulses, and τ pulse duration). In case of reciprocity, a response should increase in a linear fashion with energy density [52]. In fact, the uptake of the fluorescent tracer increased linearly for both pulses with 0.8 kV cm^{-1} and 1.6 kV cm^{-1} .

4.4. The cytoskeleton is adjacent to the plasma membrane

To observe, whether the cytoskeleton is localized in close proximity to the plasma membrane, protoplasts were generated from cells expressing either the actin-marker FABD, or the microtubule marker AthTuB6 in fusion with GFP and viewed by TIRF microscopy. Since the evanescent wave dissipates very rapidly, only the uppermost 80 nm of the cytoplasm underneath the membrane contribute to the signal. Due to the spherical shape of protoplasts, a circular area of only some $5 \mu\text{m}$ diameter can be observed. Both actin filaments (Fig. 4A,B), and microtubules (Fig. 4C) could be observed in this region. Actin filaments were organized in star-like plaques, from where finer filaments emanated. The crossings of filaments appeared as punctate structures. The pattern for microtubules appeared similar, but the star-like centers were much finer and the set-up appeared to be more delicate as compared to the actin filaments. To get insight into the topology of the submembrane cytoskeleton, z-stacks were recorded and projected

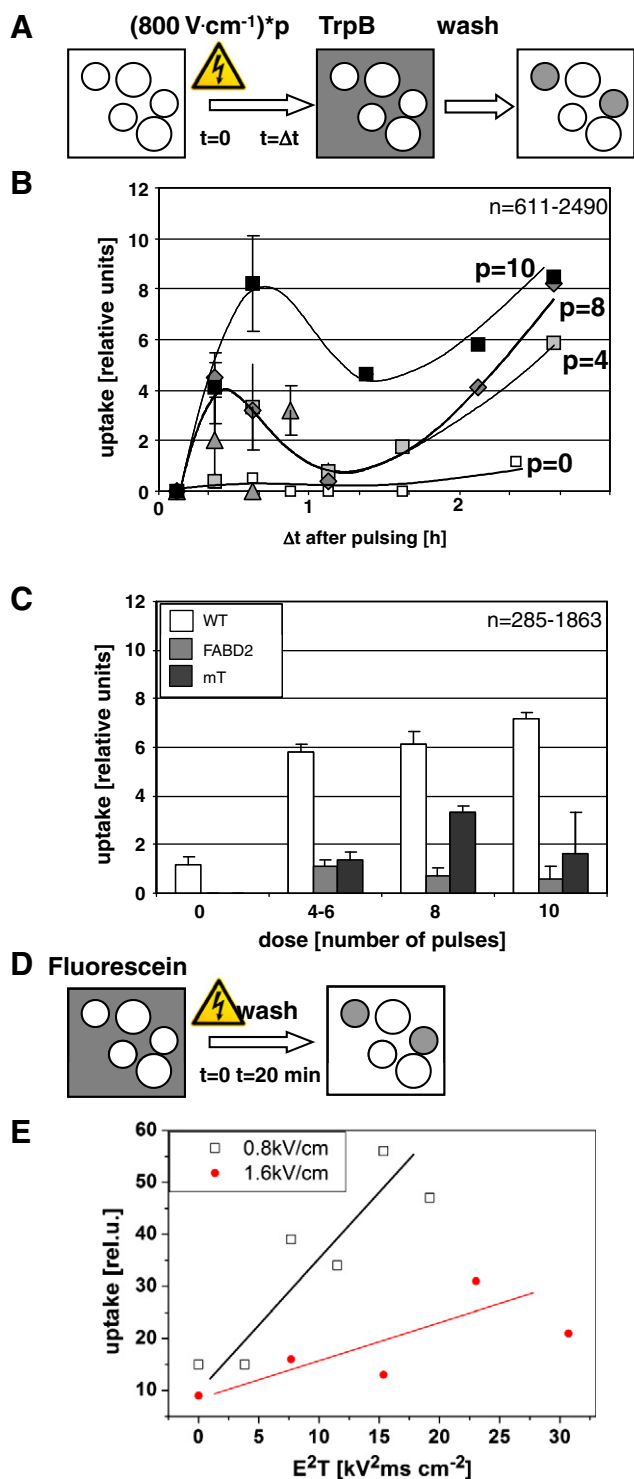


Fig. 3. Response of membrane permeability to msPEFs in tobacco protoplasts. **A** Experimental set-up to quantify uptake of Trypan Blue in response to a standard electroporation treatment. **B** Time course of membrane permeability to Trypan Blue (TrpB) using variable numbers *p* of pulses with 800 V cm⁻¹, 3 ms) in non-transformed cells of BY-2. **C** Dose response of membrane permeability to TrpB scored 2 h after pulsing. **D** Experimental set-up to quantify the uptake of Fluorescein in response to a standard electroporation treatment. **E** Dependence of membrane permeability on electric energy density for the non-toxic tracer Fluorescein present at the time of pulsing established either by pulses of 800 V cm⁻¹ (closed circles) or 1600 V cm⁻¹ (open squares).

with a tilt angle of 90° (Fig. 4D). In this projection, the actin filaments branched into finer structures towards the cell interior, whereas microtubules appeared relatively straight. The microtubule signal

reached closer towards the membrane as compared to actin. Due to the nature of TIRF microscopy it is not possible to deduce slice thickness from z-stepping intervals. Thus, in contrast to the xy-plane, the topologies in the z-direction can be represented only relatively, not in absolute dimensions.

5. Discussion

Evidence for a close link of actin with the plasma membrane is accumulating. This is expected to influence the electric properties of the plasma membrane. In fact, electric currents were reported to decrease the number of actin filaments and the decoration with actin-binding proteins in mesenchymal and osteoblast cells, accompanied by increased fluidity of the membrane [23]. In melanoma cells, actin was disrupted by nsPEFs accompanied by caspase activation and apoptosis [24]. In tobacco cells, actin filaments contracted into bundles towards the nucleus, whereas cortical microtubules disorganized and disintegrated in response to nsPEFs [25]. However, these responses of the actin cytoskeleton might be accompanying side phenomena and not causally linked with the subsequent increases of membrane permeability. To test a potential causal link, it is necessary to manipulate the cytoskeleton and to monitor, whether this will change the response of membrane permeability.

In fact, treatment with the tubulin-sequestering drug colchicine prolonged the time to recover from electroporation in mammalian cells [21,22], and pretreatment with low concentrations of phalloidin stabilized actin against nsPEFs and effectively reduced irreversible membrane leakage in tobacco cells [25]. However, pharmacological manipulation always has to deal with potential side effects – for instance, phalloidin, although binding actin with high affinity, can cause toxicity, stimulating a debate, whether additional targets might be affected as well [45]. We therefore adopted an approach based on genetic engineering by stabilizing actin through expression of actin-bundling proteins and measuring membrane permeabilization by the uptake of the membrane impermeable dye Trypan Blue. We found that permeabilization was reduced under conditions, where actin was bundled (Fig. 2C). This effect was mild for expression of FABD2, an actin-binding domain with weak bundling activity, but was strongly elevated for expression of the strong actin bundler mouse talin. Thus, the degree of membrane stabilization against electroporation correlated with the degree of actin bundling. This is corroborated by experiments, where the expression of the actin-bundling WLIM-domain is driven by a glucocorticoid-inducible promoter (Fig. 2D). In this set-up we were able to observe a glucocorticoid-inducible stabilization of membrane permeability against nsPEFs. Thus, the effect of actin bundling on membrane permeability is highly specific.

We have tested, whether this actin-dependent electrostabilization is confined to nsPEFs by testing the response of protoplasts to conventional electroporation. We observed again that uptake of fluorescent tracers after pulsing was reduced in protoplasts generated from transgenic lines expressing actin bundling proteins (Fig. 3). The uptake increased in a linear fashion with rising energy density [52] suggesting reciprocity of the biological effect.

The mechanism, by which actin stabilizes the membrane against electroporation, is far from being understood. A close interaction of actin filaments with the membrane is suggested by different lines of evidence: Treatment with phalloidin increases the amount of actin that can be copurified with plasma membranes [46], a subgroup of actin-binding formins is attached with the membrane [41,42], and the membrane-bound phospholipase D has been found to bind actin as well [43]. Using TIRF-microscopy in cells expressing GFP-tagged markers for actin and microtubules, we could image the submembraneous cytoskeleton (Fig. 4). Recently, “TIRF” imaging has been reported for walled plant cells, however, this imaging was later shown to be caused by variable angle epifluorescence (VAEF), which allows to view the uppermost few μm of a specimen without optical

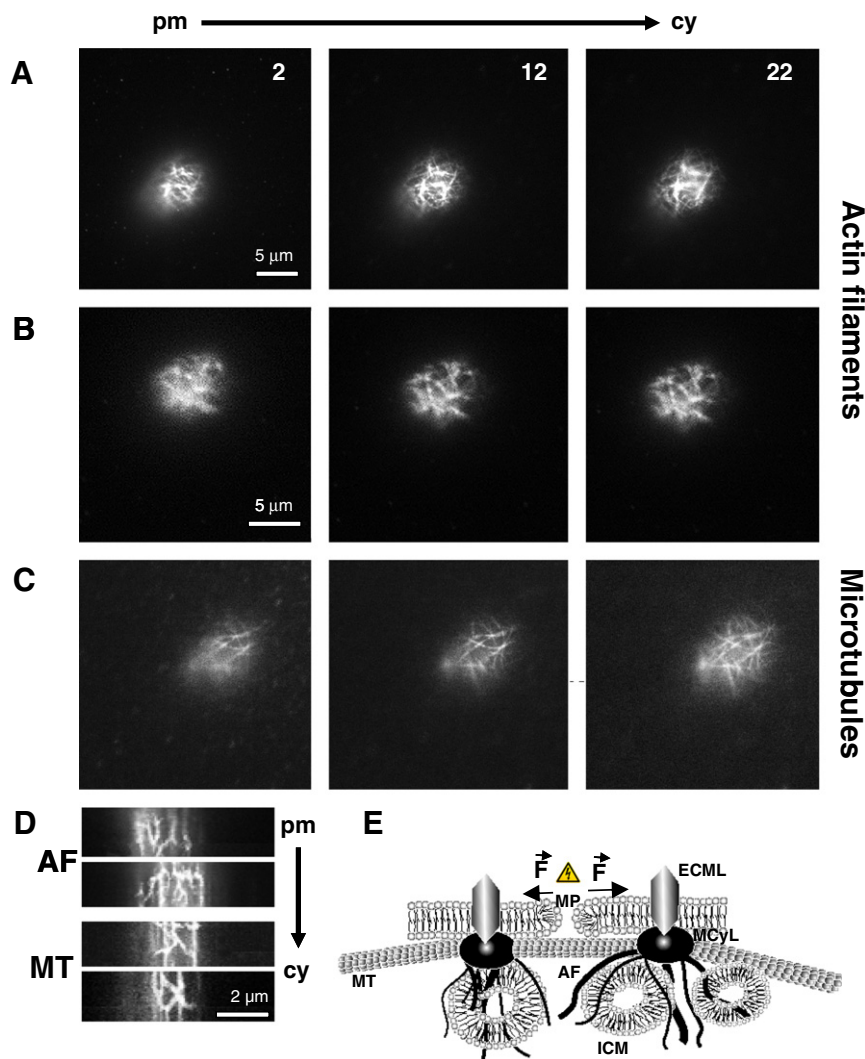


Fig. 4. Imaging of the submembrane cytoskeleton in living tobacco protoplasts using Total Internal Reflection Fluorescence Microscopy (TIRF). Actin filaments (AF) were visualized using the fimbrin actin-binding domain in fusion with GFP (A,B), microtubules (MT) using β -tubulin 6 from *Arabidopsis thaliana* in fusion with GFP (C). Individual sections of z-stacks are shown. D Orthogonal projections of z-stacks recorded by TIRF, plasma membrane (pm) oriented upwards, cytoplasm (cy) downwards. Size bar in D is valid for the xy plane, not for z axis because slice thickness cannot be deduced from z-stepping intervals. E Model for the role of actin in electropermeabilization. AF actin filaments, MT microtubules, ICM internal membrane stores, MCYL Membrane-cytoskeleton linker ECML Extracellular matrix linker MP membrane pore formed by pulsed electrical field F force vector caused by membrane tension. For simplicity, the interaction of microtubules with cellulose-synthase complexes is not depicted in the model.

bleedthrough from the deeper layer [47]. True TIRF is limited by the range of the evanescent wave generated by total reflection at the cell-glass interface and has a much lower range (<100 nm), and is characterized by a small optical field due to the curved topology of the specimen. This means that the actin filaments and microtubules visualized in our experiments are physically very close (in the range of <50 nm) to the membrane.

We observed that the apparent thickness of the plasma-membrane labeled by Trypan Blue was dependent on the degree of actin bundling (Fig. 2A). This became especially clear in a situation, when actin bundling in the talin-expressor line was rapidly downregulated by addition of exogenous auxin [48]. Concomitantly with the disappearance of massive actin cables, apparent membrane thickness decreased as well. Since the elementary membrane cannot be resolved by light microscopy, these changes of apparent thickness must be caused by membrane topologies such as tubulovesicular membrane folds or invaginations that increase membrane surface and might be structurally maintained by actin filaments (Fig. 4E).

How could the maintenance and mobilization of membrane stores contribute to a higher resistance against electropermeabilization? The

existence of such reservoirs of membrane material was already proposed several decades ago from studies with wall-free protoplasts that can swell or shrink considerably within seconds upon alterations of osmotic potential without changing their spherical shape. This phenomenon was explained by reservoirs of membrane material that can be rapidly mobilized by unfolding or exocytosis, and restored by refolding or endocytosis [49]. Since the extensibility of the plant membrane is limited, the stability of the membrane against lysis depends on the extent and mobilization of these reservoirs. We propose a model, where these submembrane are structured and possibly mobilized by actin. Whether these submembrane stores are identical to the recently identified plant-specific EXPO organelles [50], remains to be elucidated.

A link between submembrane reservoirs and resealing has also been proposed from functional studies of so called synaptotagmins. Originally identified in neurons as components for the fusion of synaptic vesicles, mutations in the plant homologues of synaptotagmins were found to affect the resilience of *Arabidopsis thaliana* to salt stress [53]. Moreover, synaptotagmin RNai plants exhibited reduced recovery from a freezing shock [54]. These observations led to a model,

where plant synaptotagmins act in the resealing of membrane damages imposed by mechanic stress, either by releasing membrane tensions through recruitment of submembrane vesicles to the damaged site, or, alternatively, by fusion of vesicle patches and subsequent fusion with the plasma membrane [55]. If synaptotagmins are involved in nsPEF-triggered resealing, downregulation by inducible RNAi in BY-2 should shift the dose–response relation for nsPEF-induced Trypan-Blue uptake towards higher pulse numbers.

How could nsPEFs trigger a reorganization of the actin cytoskeleton? The primary effect of the nsPEFs seems to be the formation of membrane pores that mediate a strong increase in potassium permeability [51]. This would decrease the potassium-dependent stabilization of actin filaments due to potassium leakage and might contribute to the observed detachment of actin from the membrane [25]. Alternatively, conformational changes of membrane-anchoring proteins such as formin 5 [41,42] or phospholipase D [43] might cause the detachment. Both possibilities are not mutually exclusive.

Interestingly, when the uptake of Trypan Blue was scored over the population of protoplasts in the electroporation experiment, permeabilization was found to be strongly non-linear. Protoplasts that did not accept any significant amount of dye coexisted with protoplasts that were heavily labeled. In the time course experiment (Fig. 3B), the strongly labeled cells died soon afterwards indicating that the highly permeable state was irreversible. The loss of these dying cells in combination with the rescue of cells that were able to reseal their pores can account for the transient decrease in the frequency of labeled cells 1 h after pulsing. By promoting the mobilization of submembrane reservoirs of membrane material, actin would relax mechanical tension on the membrane such that the pores can reseal more easily. When the formation of pores affects actin organization, for instance, by potassium leakage [51] this will, according to our model, result in a loss of these submembrane reservoirs and, thus, impede the relaxation of the pores by mobilization of these reservoirs. This will launch a self-amplificatory feedback loop that will culminate in an irreversible high-permeability state of the membrane. According to our model, bundling of actin will stabilize actin against potassium leakage and/or detachment from membrane anchoring proteins and thus interrupt this feedback loop channeling the membrane response towards membrane relaxation and resealing of the pores.

6. Conclusions

We have investigated the role of the actin cytoskeleton for the response of plant cells to nsPEFs and to long pulses typically utilized for classical electroporation. By engineering different degrees of actin bundling and measuring membrane permeability by the uptake of Trypan Blue we can show that actin bundling stabilizes the membrane against electroporation. Using a glucocorticoid inducible promoter driving an actin bundling protein domain we can manipulate the resistance against electroporation by the glucocorticoid dexamethasone. We observe changes in apparent membrane thickness that depend on actin bundling and we can show by TIRF microscopy that actin and microtubules are in close physical contact (<50 nm) with the membrane. We propose a model, where the plasma membrane is in a dynamic equilibrium with a submembrane tubulovesicular reservoir of membrane material that is maintained and mobilized by actin filaments and that contributes to the resealing of pores induced by nsPEFs through relaxation of mechanic tensions in the membrane.

Acknowledgments

This work was supported by the Excellency Program of the KIT (Shared Research Group SRG60-1). We gratefully acknowledge the kind gift of the Lifeact–VENUS construct by Dr. Tsuyoshi Nakagawa (Shimane University, Japan), of the GFP–talin cell line by Dr. Jan Petrášek (Institute of Experimental Botany, Czech Academy of Sciences, Prague), of the

glucocorticoid-inducible WLIM line by Dr. André Steinmetz (Centre de Recherche Public-Santé, Luxembourg), of the FABD2 line by Dr. Jan Maisch (Botanical Institute, Karlsruhe Institute of Technology, Germany), and of the AtTuB6 line by Dr. Kateřina Schwarzerová (Department of Plant Physiology, Charles University, Prague, Czech Republic). We thank Sabine Purper (Botanical Institute, Karlsruhe Institute of Technology, Germany) for competent cultivation of high-quality cell lines.

References

- [1] J. Teissie, M. Golzio, M.P. Rols, Mechanisms of cell membrane electroporation: a minireview of our present (lack of ?) knowledge, *BBA* 1724 (2005) 270–280.
- [2] J.C. Weaver, Y.A. Chizmadzhev, Electroporation, in: C. Polk, E. Postow (Eds.), *Handbook of Biological Effects of Electromagnetic Fields*, second ed., CRC Press, Boca Raton, FL, 1996, pp. 247–274.
- [3] U. Zimmermann, G.A. Neil, *Electromanipulation of Cells*, CRC Press, Boca Raton, FL, 1996.
- [4] E. Neumann, S. Kakorin, T. Toensing, Fundamentals of electroporative delivery of drugs and genes, *Bioelectrochem. Bioenerg.* 48 (1999) 3–16.
- [5] M. Sack, J. Sigler, S. Frenzel, Chr. Eing, J. Arnold, Th. Michelberger, W. Frey, F. Attmann, L. Stukenbrock, G. Mueller, Research on industrial-scale electroporation devices fostering the extraction of substances from biological tissue, *Food Eng. Rev.* 2 (2) (2010) 147–156.
- [6] D. Knorr, A. Angersbach, M.N. Eshtiagi, V. Heinz, D. Lee, Processing concepts based on high intensity electric field pulses, *Trends Food Sci. Technol.* 12 (2001) 129–135.
- [7] N. Lebovka, M. Bazhal, E. Vorobiev, Simulation and experimental investigation of food material breakage using pulsed electric field treatment, *J. Food Eng.* 44 (2000) 213–223.
- [8] A.J.H. Sale, W.A. Hamilton, Effects of high electric fields on microorganisms. I. Killing of bacteria and yeasts, *Biochim. Biophys. Acta* 148 (1967) 781–788.
- [9] C. Gusbeth, W. Frey, H. Volkmann, T. Schwartz, H. Bluhm, Pulsed electric field treatment for bacteria reduction and its impact on hospital wastewater, *Chemosphere* 75 (2009) 228–233.
- [10] S. Toepfl, V. Heinz, D. Knorr, High intensity pulsed electric fields applied for food preservation, *Chem. Eng. Process.* 46 (2007) 537–546.
- [11] P.C. Wouters, I. Alvarez, J. Raso, Critical factors determining inactivation kinetics by pulsed electric field food processing, *Trends Food Sci. Technol.* 12 (2001) 112–121.
- [12] C. Chen, S.W. Smye, M.P. Robinson, J.A. Evans, Membrane electroporation theories: a review, *Med. Biol. Eng. Comput.* 44 (2006) 5–14.
- [13] K.H. Schoenbach, R.P. Joshi, J. Kolb, N. Chen, M. Stacey, P. Blackmore, E.S. Buescher, S.J. Beebe, Ultrashort electrical pulses open a new gateway into biological cells, *Proc. IEEE* 92 (2004) 1122–1137.
- [14] S.S. Scarlett, J.A. White, P.F. Blackmore, K.H. Schoenbach, J.F. Kolb, Regulation of intracellular calcium concentration by nanosecond pulsed electric fields, *BBA-Biomembranes* 1788 (2009) 1168–1175.
- [15] P.T. Vernier, Y. Sun, L. Marcu, S. Salemi, C.M. Craft, M.A. Gundersen, Calcium bursts induced by nanosecond electric pulses, *Biochem. Biophys. Res. Commun.* 310 (2003) 286–295.
- [16] P.T. Vernier, M.J. Ziegler, Y. Sun, W.V. Chang, M.A. Gundersen, D.P. Tieleman, Nanopore formation and phosphatidylserine externalization in a phospholipid bilayer at high transmembrane potential, *J. Am. Chem. Soc.* 128 (2006) 6288–6289.
- [17] S.J. Beebe, P.M. Fox, L.J. Rec, E.L. Willis, K.H. Schoenbach, Nanosecond, high-intensity pulsed electric fields induce apoptosis in human cells, *FASEB J.* 17 (2003) 1493–1495.
- [18] X. Chen, J.F. Kolb, R.J. Swanson, K.H. Schoenbach, S.J. Beebe, Apoptosis initiation and angiogenesis inhibition: melanoma targets for nanosecond pulsed electric fields, *Pigment Cell Melanoma Res.* 23 (2010) 554–563.
- [19] R. Nuccitelli, U. Pliquet, X. Chen, W. Ford, J.R. Swanson, S.J. Beebe, J.F. Kolb, K.H. Schoenbach, Nanosecond pulsed electric fields cause melanomas to self-destruct, *Biochem. Biophys. Res. Commun.* 343 (2006) 351–360.
- [20] J. Pokorny, J. Hasek, F. Jelinek, Endogenous electric field and organization of living matter, *Electromagn Biol Med* 24 (2005) 185–197.
- [21] M.P. Rols, J. Teissie, Experimental evidence for the involvement of the cytoskeleton in mammalian cell electroporation, *Biochim Biophys Acta* 1111 (1992) 45–50.
- [22] J. Teissie, M.P. Rols, Manipulation of cell cytoskeleton affects the lifetime of cell membrane electroporation, *Ann. N. Y. Acad. Sci.* 720 (1994) 98–110.
- [23] I. Titushkin, M. Cho, Regulation of cell cytoskeleton and membrane mechanics by electric field: role of linker proteins, *Biophys. J.* 96 (2009) 717–728.
- [24] W.E. Ford, W. Ren, P.F. Blackmore, K.H. Schoenbach, S.J. Beebe, Nanosecond pulsed electric fields stimulate apoptosis without release of pro-apoptotic factors from mitochondria in B16f10 melanoma, *Arch. Biochem. Biophys.* 497 (2010) 82–89.
- [25] Th. Berghöfer, C. Eing, B. Flickinger, P. Hohenberger, L. Wegner, W. Frey, P. Nick, Nanosecond electric pulses trigger actin responses in plant cells, *Biochem. Biophys. Res. Commun.* 387 (2009) 590–595.
- [26] T. Nagata, Y. Nemoto, S. Hasezawa, Tobacco BY-2 cell line as the 'Hela' cell in the cell biology of higher plants, *Int. Rev. Cytol.* 132 (1992) 1–30.

- [27] J. Maisch, J. Fišerová, L. Fischer, P. Nick, Actin-related protein 3 labels actin-nucleating sites in tobacco BY-2 cells, *J. Exp. Bot.* 60 (2009) 603–614.
- [28] B. Kost, P. Spielhofer, N.H. Chua, A GFP-mouse talin fusion protein labels plant actin filaments *in vivo* and visualizes the actin cytoskeleton in growing pollen tubes, *Plant J.* 16 (1998) 393–401.
- [29] C. Thomas, F. Moreau, M. Dieterle, C. Hoffmann, S. Gatti, C. Hofmann, M. Van Troys, C. Ampe, A. Steinmetz, The LIM Domains of WLLIM1 define a new class of actin bundling modules, *J. Biol. Chem.* 282 (2007) 33599–33608.
- [30] A. Era, M. Tominaga, K. Ebine, Ch. Awai, Ch. Saito, K. Ishizaki, K.T. Yamato, T. Kohchi, A. Nakano, T. Ueda, Application of Lifeact Reveals F-Actin Dynamics in *Arabidopsis thaliana* and the Liverwort, *Marchantia polymorpha*, *Plant Cell Physiol.* 50 (2009) 1041–1048.
- [31] M. Nakamura, K. Naoi, T. Shoji, T. Hashimoto, Low concentrations of propyzamide and oryzalin alter microtubule dynamics in arabidopsis epidermal cells, *Plant Cell Physiol.* 45 (2004) 1330–1334.
- [32] T. Dansako, K. Kato, J. Satoh, M. Sekine, K. Yoshida, A. Shinmyo, 5' untranslated region of the HSP18.2 gene contributes to efficient translation in plant cells, *J. Biosci. Bioeng.* 95 (2003) 52–58.
- [33] V.E. Franklin-Tong, C.W. Goutay, A role for actin in regulating apoptosis/programmed cell death: evidence spanning yeast, plants and animals, *Biochem. J.* 413 (2008) 389–404.
- [34] B. Geiger, A. Bershadsky, Assembly and mechanosensory function of focal contacts, *Curr. Opin. Cell Biol.* 13 (2001) 584–592.
- [35] F.G. Giancotti, E. Ruoslahti, Integrin signaling, *Science* 285 (1990) 1028–1032.
- [36] H. Canut, A. Carrasco, J.P. Galaud, C. Cassan, H. Bouyssou, N. Vita, P. Ferrara, R. Pont-Lezica, High affinity RGD-binding sites at the plasma membrane of *Arabidopsis thaliana* link the cell wall, *Plant J.* 16 (1998) 63–71.
- [37] J. Zhou, B. Wang, Y. Li, Y. Wang, L. Zhu, Responses of *Chrysanthemum* cells to mechanical stimulation require intact microtubules and plasma membrane-cell wall adhesion, *J. Plant Growth Regul.* 26 (2007) 55–68.
- [38] M.L. Coleman, E.A. Sahai, M. Yeo, M. Bosch, A. Dewar, M.F. Olson, Membrane blebbing during apoptosis results from caspase-mediated activation of ROCK I, *Nat. Cell Biol.* 3 (2001) 339–345.
- [39] K. Takano, K. Toyooka, Sh. Suetsugu, EFC/F-BAR proteins and the N-WASP–WIP complex induce membrane curvature-dependent actin polymerization, *EMBO J.* 27 (2008) 2817–2828.
- [40] T. Higaki, T. Sano, S. Hasezawa, Actin microfilament dynamics and actin side-binding proteins in plants, *Curr. Opin. Plant Biol.* 10 (2007) 549–556.
- [41] A.Y. Cheung, Sh. Niroomand, Y. Zou, H.M. Wu, A transmembrane formin nucleates subapical actin assembly and controls tip-focused growth in pollen tubes, *Proc. Natl. Acad. Sci. U. S. A.* 107 (2010) 16390–16395.
- [42] Zh. Zhang, Y. Zhang, H. Tan, Y. Wang, G. Li, W. Liang, Zh. Yuan, J. Hu, H. Ren, D. Zhang, Rice morphology determinant encodes the type II formin FH5 and regulates rice morphogenesis, *Plant Cell* (2011), doi:10.1105/tpc.110.081349 published online.
- [43] R. Pleskot, M. Potocký, P. Pejchar, J. Linek, R. Bezvoda, J. Martinec, O. Valentová, Z. Novotná, V. Žárský, Mutual regulation of plant phospholipase D and the actin cytoskeleton, *Plant J.* 62 (2010) 494–507.
- [44] J.C. Gardiner, J.D. Harper, N.D. Weerakoon, D.A. Collings, S. Ritchie, S. Gilroy, R.J. Cyr, J. Marc, A 90-kD phospholipase D from tobacco binds to microtubules and the plasma membrane, *Plant Cell* 13 (2001) 2143–2158.
- [45] J.A. Cooper, Effects of cytochalasin and phalloidin on actin, *J. Cell Biol.* (1987) 1473–1478.
- [46] G. Gabbiani, R. Montesano, B. Tuchweber, M. Salas, L. Orci, Phalloidin-induced hyperplasia of actin filaments in hepatocytes, *Lab. Invest.* 33 (1975) 562.
- [47] I.A. Sparkes, K. Graumann, A. Martinière, J. Schoberer, P. Wang, A. Osterrieder, Bleach it, switch it, bounce it, pull it: using lasers to reveal plant cell dynamics, *J. Exp. Bot.* 62 (2011) 1–7.
- [48] J. Maisch, P. Nick, Actin is involved in auxin-dependent patterning, *Plant Physiol.* 143 (2007) 1695–1704.
- [49] J. Wolfe, M.F. Dowgert, P.L. Steponkus, Mechanical study of the deformation and rupture of the plasma membranes of protoplasts during osmotic expansions, *J. Membr. Biol.* 93 (1986) 63–74.
- [50] J. Wang, Y. Ding, J. Wang, S. Hillmer, Y. Miao, S.W. Lo, X.F. Wang, D.G. Robinson, L.W. Jiang, EXPO, an exocyst-positive organelle distinct from multivesicular endosomes and autophagosomes, mediates cytosol to cell wall exocytosis in arabidopsis and tobacco cells, *Plant Cell* 22 (2010) 4009–4030.
- [51] L.H. Wegner, B. Flickinger, C. Eing, T. Berghöfer, P. Hohenberger, W. Frey, P. Nick, A patch clamp study on the electro-permeabilization of higher plant cells: Supra-physiological voltages induce a high-conductance, K(+) selective state of the plasma membrane, *BBA Membranes* 1808 (2011) 1728–1736.
- [52] K.H. Schoenbach, R.P. Joshi, S.J. Beebe, A scaling law for membrane permeabilization with nanopulses, *IEEE Trans. Dielectr. Electr. Insul.* 16 (2009) 1224–1234.
- [53] A.L. Schapire, B. Voigt, J. Jasik, A. Rosado, R. Lopez-Cobollo, D. Menzel, J. Salinas, S. Mancuso, V. Valpuesta, F. Baluška, M.A. Botella, Arabidopsis synaptotagmin 1 is required for the maintenance of plasma membrane integrity and cell viability, *Plant Cell* 20 (2008) 3374–3388.
- [54] T. Yamazaki, Y. Kawamura, A. Minami, M. Uemura, Calcium-dependent freezing tolerance in Arabidopsis involves membrane resealing via synaptotagmin SYT1, *Plant Cell* 20 (2008) 3389–3404.
- [55] A.L. Schapire, V. Valpuesta, M.A. Botella, Plasma membrane repair in plants, *Trends Plant Sci.* 14 (2009) 645–652.